BIOLOGY OF REPRODUCTION (2012) **87**(5):125, 1–11
Published online before print 5 September 2012.
DOI 10.1095/biolreprod.112.102830

Imaging of Vascular Development in Early Mouse Decidua and Its Association with Leukocytes and Trophoblasts[1]

B. Anne Croy,[2,3,4] Zhilin Chen,[3,4] Alexander P. Hofmann,[4] Edith M. Lord,[5] Abigail L. Sedlacek,[5] and Scott A. Gerber[5]

[4]*Department of Biomedical and Molecular Sciences, Queen's University, Kingston, Ontario, Canada*
[5]*Department of Microbiology and Immunology, University of Rochester Medical Center, Rochester, New York*

ABSTRACT

In species with endometrial decidualization and hemochorial placentation (humans, mice, and others), leukocytes localize to early implant sites and contribute to decidual angiogenesis, spiral arterial remodeling, and trophoblast invasion. Relationships between leukocytes, trophoblasts, and the decidual vasculature are not fully defined. Early C57BL/6J implant sites were analyzed by flow cytometry to define leukocyte subsets and by whole-mount immunohistochemistry to visualize relationships between leukocytes, decidual vessels, and trophoblasts. Ptprc$^+$ (CD45$^+$) cells increased in decidua between Gestational Day (GD) 5.5 and GD 9.5. Uterine natural killer (uNK) cells that showed dynamic expression of Cd (CD) 69, an activating receptor, and Klrg1 (KLRG1), an inhibitory receptor, localized mesometrially and were the dominant CD45$^+$ cells between GD 5.5 and GD 7.5. At GD 8.5, immature monocytes that occurred throughout decidua exceeded uNK cells numerically and many leukocytes acquired irregular shapes, and leukocyte-leukocyte conjugates became frequent. Vessels were morphologically heterogeneous and regionally unique. Migrating trophoblasts were first observed at GD 6.5 and, at GD 9.5, breached endothelium, entered vascular lumens, and appeared to occlude some vessels, as described for human spiral arteries. No leukocyte-trophoblast conjugates were detected. Whole-mount staining gave unparalleled decidual vascular detail and cell-specific positional information. Its application across murine models of pregnancy disturbances should significantly advance our understanding of the maternal-fetal interface.

angiogenesis, conceptus, decidua, immunology, pregnancy, trophoblast

INTRODUCTION

In species with hemochorial placentation, blastocyst implantation initiates massive structural changes in the uterus that continue across pregnancy and are synchronized with conceptus development. Early endometrial changes include loss of uterine lumen epithelium at implant sites, decidualization of endometrial stromal cells, neoangiogenesis, leukocyte recruitment, and invasion of trophoblasts from the developing fetal placental primordium [1–3]. Most human gestational complications are linked to deviations in one or more of these processes [4–7]. For example, deficits in molecules such as placenta growth factor (PGF) and excesses of antiangiogenic molecules such as soluble vascular endothelial cell growth factor receptor-1 (sFLT1) occur in preeclampsia, a syndrome that affects approximately 5% of all human pregnancies and that may include limited intravascular trophoblast invasion and intrauterine fetal growth restriction [4]. Angiogenic cells of many lineages are present in implant sites [8–12] and, in mice, include uterine natural killer (uNK) cells (the most abundant leukocytes in early decidua), macrophages, dendritic cells (DCs), and trophoblasts. These cell types produce proangiogenic factors, including vascular endothelial growth factor A (VEGFA), angiopoietins, and PGF [13, 14].

Lymphocyte-promoted angiogenesis is recognized in pathological conditions such as cardiac infarcts, vascular grafts, and tumor growth [15–18]. In these disease models and in normal tissues such as the developing fetus and neonatal retina, understanding of vasculogenesis, angiogenesis, and vessel remodeling has been advanced by whole-mount in situ hybridization and by whole-mount immunohistochemical staining of samples from normal and mutant mice [19–21]. In the present study, we apply the techniques of flow cytometry and whole-mount immunohistochemistry to early normal mouse decidua and report previously unrecognized changes in leukocyte subset proportions as well as dynamic expression of a selected pair of leukocyte activation and inhibitory receptors. In addition, we define the normal positional relationships between leukocytes, trophoblasts, and the vasculature from implantation (Gestational Day [GD] 4.5) to the onset of placental circulation (GD 9.5). By use of whole-mount staining, superior resolution of the heterogeneity and complexity of early decidual microvessels was obtained. Leukocyte-enriched decidua basalis was the most richly vascularized region. The earliest stages of trophoblast invasion into decidua were clearly visualized, as were the precise times for widespread leukocyte activation and for trophoblasts crossing the endothelium and entering vessel lumens.

MATERIALS AND METHODS

Animals

C57BL/6 (B6) mice were purchased from Charles River Canada (for use at Queen's University) or The Jackson Laboratory (for use at the University of Rochester). B6-Tg (UBC-GFP)/30SchaJ (*Gfp*$^{+/-}$) mice from The Jackson Laboratory were bred to be homozygous *Gfp*/*Gfp* mice at Queen's University. For flow cytometry, at least three B6 females mated by B6 males were studied on each of GD 5.5, 6.5, 7.5, 8.5, and 9.5. For whole-mount staining, B6 female virgins (n = 5; estrous cycle dated by ovarian gross morphology and vaginal smear) or females mated to syngeneic normal or *Gfp*/*Gfp* males were studied (copulation plug = GD 0.5). Pregnancies were studied at GD 4.5, 5.0, 5.5, 6.5, 7.5, 8.5, and 9.5, with from two to five pregnancies per time point. Mice were

[1]Supported by Awards from the NSERC, CIHR, CFI, and Canada Research Chairs Program to B.A.C. and from the NIH to E.M.L.
[2]Correspondence: Anne Croy, Department of Biomedical and Molecular Sciences, Queen's University, Kingston, ON K7L 3N6, Canada. E-mail: croya@queensu.ca
[3]These authors contributed equally to this study.

Received: 15 June 2012.
First decision: 13 July 2012.
Accepted: 29 August 2012.

eISSN: 1529-7268 http://www.biolreprod.org
ISSN: 0006-3363

euthanized by cervical dislocation, and uteri were removed and dissected as described below. All animal usage was covered by approved animal utilization procedures at the respective institutions.

Fluorescence-Activated Cell Sorting Analyses

For fluorescence-activated cell sorting (FACS) analyses, decidual capsules were removed from the uterine wall, and five (or more for GD 5.5) littermate implant sites were pooled. Conceptuses were not removed. Deciduas were processed into single-cell suspensions using a modification of a previously published technique [22]. Briefly, tissues were finely minced in 0.2% collagenase D (Sigma Chemical) in Hanks balanced salt solution, incubated (37°C, 45 min, rocking), filtered (mesh size, 40 μm) into PBS supplemented with 1% bovine serum albumin and 0.1% sodium azide (PBA), counted, washed (PBA, 4°C, 300 × *g*), and resuspended at 1×10^6 cells per 100 μl per flow cytometry tube in PBA. Samples were blocked using anti-CD16/CD32 (supernatant of hybridoma 2.4G2; American Type Culture Collection), followed by the addition of primary antibodies (0.5 μg/ml) for a 30-min incubation on ice. The antibodies used in flow cytometry and in the whole-mount analyses are given in Supplementary Table S1 (all Supplemental Data are available online at www.biolreprod.org). Next, cells were washed by centrifugation (5 min, 4°C, 300 × *g*) in 1 ml of PBA and resuspended in 300 μl of PBA for data collection using an eight-color FACSCanto cytometer (BD, Franklin Lakes, NJ) using fluorescence minus one (FMO) as controls. Samples were analyzed using FloJo software (Treestar).

Whole-Mount Staining

Dissections. Uterine dissections for whole-mount staining were conducted under dissection microscope magnification (25×–50×) and varied by GD. Virgin and GD 4.5 uteri were bisected at the cervix, after which, using a scalpel, each horn was halved in length and then cut from either the mesometrial to antimesometrial side or transversely to separate the mesometrial from the antimesometrial side. Tissues were then placed into PBA on ice. For GD 5.0–9.5, when implant sites could be discriminated, uteri were dissected into individual implant sites. For GD 5.0 and GD 5.5, each implant site was transected in half (i.e., the uterine wall was not removed). From GD 6.5 to GD 9.5, the uterine wall was incised along the antimesometrial border using no. 5 watchmaker forceps (Fine Science Tools), reflected over the mesometrial side, and trimmed using a razor blade to leave only a small skirt of mesometrial myometrium at the decidual attachment site as a landmark. GD 6.5–9.5 decidual capsules were then halved midsagittally or transversely under dissection microscopy with the goal of exposing the embryonic crypt. Dissections are shown in Supplementary Figure S1A. Rare resorption sites were excluded from the study.

Procedure. Whole-mount staining was performed as previously described [20]. Briefly, dissected tissue was incubated in 200 μl of PBA in a 5-ml tube along with 10 μg/ml of blocking antibody to the immunoglobulin (Ig) G Fc receptor (anti-CD16/CD32; supernatant of hybridoma 2.4G2) and 5–10 μg/ml of fluorescent-conjugated (fluorescein isothiocyanate [FITC], phycoerythrin [PE], or allophycocyanin [APC]) primary antibodies.

Paraffin Section Histology

To support the interpretations of whole-mount staining, sections (6 μm thick) were prepared from archived, GD-matched, paraffin-embedded blocks of perfusion-fixed (4% paraformaldehyde) B6 uteri and stained using routine protocols for hematoxylin and eosin (H&E) or lectin *Dolichos biflorus* agglutinin (DBA) [23].

Morphometric Studies and Statistics

One-way ANOVA was used to compare differences in flow cytometric mean fluorescence intensity (MFI) over time within a particular cell population; a *P*-value of less than 0.05 was deemed to be significant. For measurement of vessels and trophoblast migration, tissue images were divided into 12 numbered quadrants. A random number generator was used to select four different grid boxes in which all the vessels were measured for width. Edge endothelial cells were traced, and Image J software (Media Cybernetics, Inc.) was used to calculate the average distance between the walls of the vessels. Images of implant sites from two or three different uteri were used to calculate mean vessel width using 17–19 measurements taken within a similar decidual region. To address vessel branching, the same randomization process was used, and within selected grids, each branch point in the same visual plane was counted in images collected at 100× magnification. One-way ANOVA was used to compare values, with a *P*-value of less than 0.05 again considered to be significant. Trophoblast invasion distance was measured from either embryonic pole and from the lateral side of the conceptus in a straight line to the furthest detectable trophoblast cell. This measure was not compared between implant sites due to variability in angles of cuts and in exact embryonic developmental stage both within and between litters.

RESULTS

FACS Analyses of Leukocyte Subsets in GD 5.5–9.5 Mouse Decidua

To identify leukocyte subsets present in early pregnancy, decidua (visible from GD 5.5) were peeled from the uterine wall and dissociated (without conceptus removal) into single-cell suspensions for flow cytometric analyses. Grossly, decidual sizes increased as pregnancy progressed. This was reflected in the increasing total cell yields per decidua (including conceptus; data not shown) and in increasing $Ptprc^+$ ($CD45^+$) cell yields per decidua (Supplementary Fig. S2A) between GD 5.5 and GD 9.5. These developmental times precede fetal leukocyte development. Leukocyte subsets were expressed as percentage of $CD45^+$ cells (Fig. 1A). At GD 5.5, NK cells ($Cd3e^-$ $Klrb1c^+$ ($CD3^-NK1.1^+$)) were the dominant subset, representing 50% of total $CD45^+$ cells. NK cell percentages decreased in whole decidua over time, and by GD 9.5 (midpregnancy), $NK1.1^+$ NK cells were 10%–15% of total $CD45^+$ cells. A population possessing monocyte-like surface markers ($Emr1^-$, $Itgax^-$, $Ly6g^-$, $Itgam^+$ ($F4/80^-$, $CD11c^-$, $Gr\text{-}1^-$, $CD11b^+$)) was fourth in abundance at GD 5.5; second in abundance at GD 6.5 and GD 7.5, and the dominant leukocyte population at GD 8.5 and GD 9.5. Importantly, this population did not express myeloid-derived suppressor cell markers such as Gr-1. A small percentage (2.7%) of the $F4/80^-$, $CD11c^-$, $Gr\text{-}1^-$, $CD11b^+$ cells expressed the eosinophil marker Siglec5 (sIglec-F) [24]. Macrophages and DCs each composed 15%–20% of total $CD45^+$ cells, and their proportions were stable over the study interval. Less abundant populations were also relatively stable between GD 5.5 and GD 9.5 and present in the declining order of $Cd19^+$ ($CD19^+$) B cells (3%–10%), granulocytes (<5%), $Cd4^+$ ($CD4^+$) T cells (<2%), and $Cd8^+$ ($CD8^+$) T cells (<2%). The proportion of B cells increased from approximately 5% to approximately 20%–25% at GD 9.5.

Activation status was examined in selected lymphocyte subsets. The early activation marker CD69 was highly expressed by all GD 5.5 and GD 6.5 uNK cells, then CD69 MFI declined (Fig. 1B). At all times, most uNK cells expressed high levels of the inhibitory surface receptor KLRG1 (Fig. 1C). Importantly, MFI indicated that KLRG1 levels on reactive uNK cells increased significantly with gestation. These data suggest an inverse correlation between the activation marker CD69 and the inhibitory marker, KLRG1, on uNK cells. CD69 was expressed at minimal levels on $CD4^+$ and on $CD8^+$ T cells (Fig. 1B). KLRG1 levels on $CD8^+$ T cells also increased with advancing gestation, but in the case of $CD8^+$ T cells, a change in the percentage of $KRLG1^+$ cells, which increased from approximately 5% to approximately 40%, was responsible for the overall increase in MFI rather than MFI per cell (Fig. 1C).

Whole-Mount Analyses

Cycling uterus. To address whether whole-mount staining would resolve vessels of the adult mouse uterus and to define potential landmark features, staining with anti-Pecam1 (CD31), a marker predominately on endothelium of blood and lymphatic vessels, was applied to longitudinally cut horns from cycling uteri. Serosal (external uterine surface) vessels

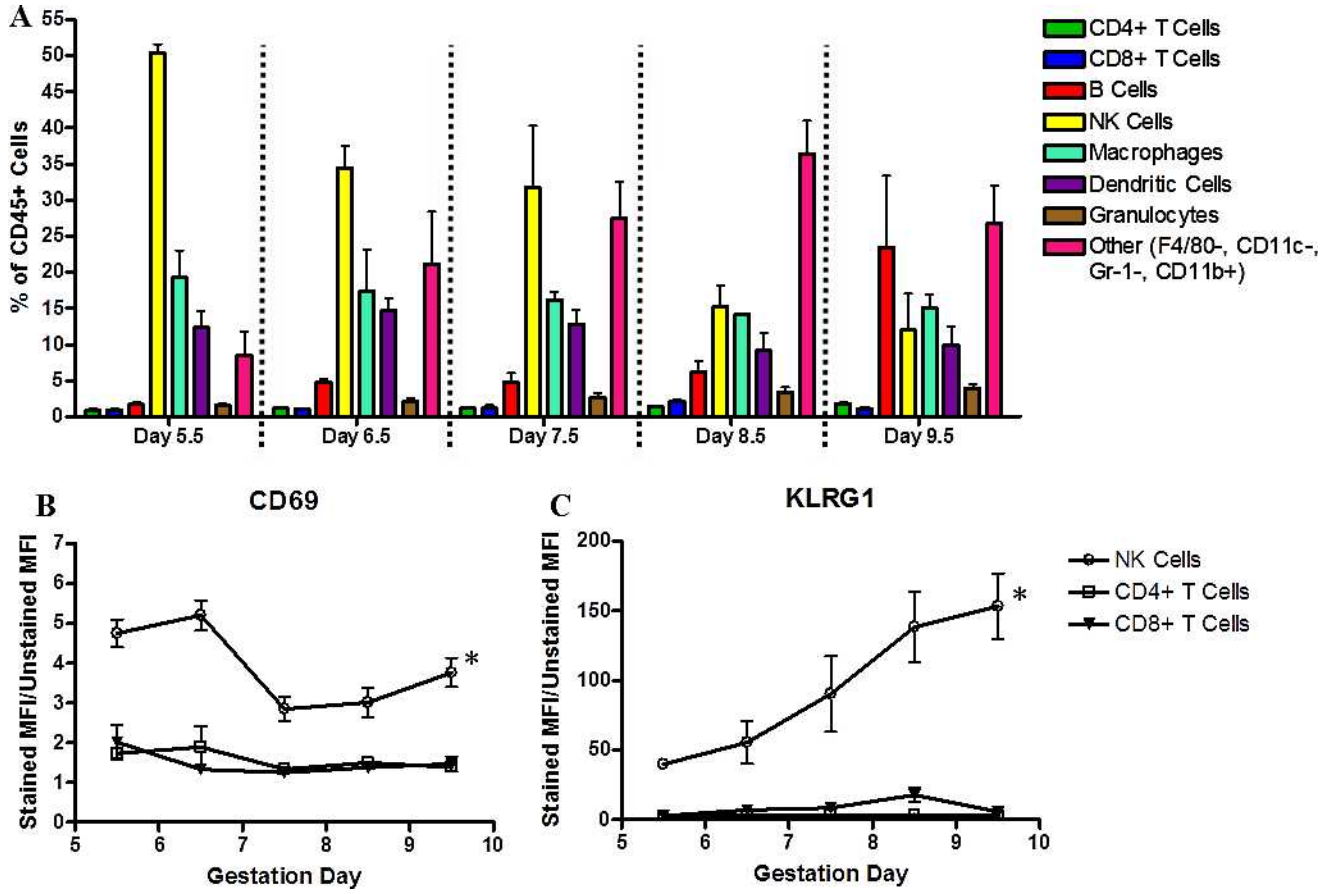

FIG. 1. Analyses of immune subsets in GD 5.5–9.5 decidua. Timed gestational decidua were processed into single-cell suspensions and stained with fluorescent-conjugated antibodies to delineate immune cell subsets and activation status. All data were first gated for $CD45^+$ cells and are expressed as the percentage of $CD45^+$ cells (**A**). Immune cell subsets were defined as follows: $CD4^+$ or $CD8^+$ T cells; $CD19^+$ B cells; $NK1.1^+$ NK cells; $F4/80^+$, $CD11b^+$ macrophages; $F4/80^-$, $CD11b^+$, $CD11c^+$ DCs; $F4/80^-$, $GR\text{-}1^+$ granulocytes; and $F4/80^+$, $CD11b^+$, $CD11c^-$, Gr-1- monocyte-like cells. The activation markers, CD69 (**B**) and KLRG1 (**C**), were used to examine lymphocytes and are expressed as MFI for each cell population. Experiments were repeated three times per time point; data are presented are the mean ± SEM from the replicate experiments. An asterisk indicates significance ($P < 0.05$) as determined by a one-way ANOVA comparing differences in MFI over time within a particular cell population.

served as landmarks. These vessels were relatively straight, long, and appeared to be longitudinally aligned with external uterine wall muscles (Fig. 2Ai). This alignment was confirmed using paraffin-embedded, H&E-stained sections (Fig. 2Aii). Wider, blunt-ended vessels were seen deeper in the uterine wall (myometrium) (arrowheads in high-power inset of Fig. 2Ai). These vessels were confirmed to be lymphatic using anti-Lyve1 (LYVE-1) antibody staining (data not shown).

The uterine mucosal (lumen) surface was highly folded in stained, unfixed whole mounts (Fig. 2Bi) and in histological sections of fixed uteri (Fig. 2Bii). Mucosal vessels were more varied structurally than serosal vessels and distinct from them. No lymphatic-like vessels were observed from the mucosal side. In specimens stained for CD45, leukocytes were evident across the uterine mucosa (data not shown).

Gestational Days 4.5 and 5.0. By GD 4.5, mouse blastocysts have hatched from the zona pellucida, elongated, and attached to the antimesometrial uterine wall, stimulating the process of uterine lumen closure [25]. In GD 4.5 whole-mount specimens, GFP-tagged conceptuses were readily detected by their green fluorescence. The GFP signal occurred across the embryo and provided definition of embryonic structures (Fig. 3). The $Gfp^{+/-}$ had no leukocyte-enrichment (Fig. 3A). Vessels appeared to be stable and without evidence for initiation of angiogenesis (Fig. 3B), but uterine lumen closure had advanced (compare asterisk in Fig. 3A to that in Fig. 2Bi). Angiogenesis began within the next 12 h and was recognized as an increase in the number of vessels and a morphologic change in $CD31^+$ endothelial cell edges (blebbing). Blebbing was interpreted as endothelial tip cell differentiation and sprouting from preexisting vessels. Sprouting angiogenesis (arrowheads in Fig. 3D) was widespread and appeared to radiate from the $Gfp^{+/-}$ conceptus at the center of each implant site (Fig. 3, C [arrows] and D) towards ablumenal regions not yet showing signs of vascular change. At GD 4.5 and GD 5.0, no GFP-expressing trophoblast cells appeared to be detached from conceptuses and invading amongst the five litters examined.

Gestational Days 5.5–7.5. From GD 5.5, implant sites can be recognized grossly as decidual swellings and dissected. GD 5.5–7.5 sites enlarge primarily by decidual rather than conceptus growth (Fig. 4A, GD 6.5). Whole-mount staining of GD 5.5–7.5 implant sites showed expected features defined previously by standard histological methods (Fig. 4A). Implantation chambers containing conceptuses enlarged, residual uterine lumens diminished, and $CD45^+$ cells became enriched mesometrially. Whole-mount staining suggested a stronger relationship between $CD45^+$ cells and myometrium than conventional histology and provided a two-dimensional perspective of a leukocyte ''cloud'' in decidua basalis (Fig. 4B). $CD45^+$ cells were present outside of the cloud but at lower cell frequencies (Fig. 4B). Surfaces lining the implan-

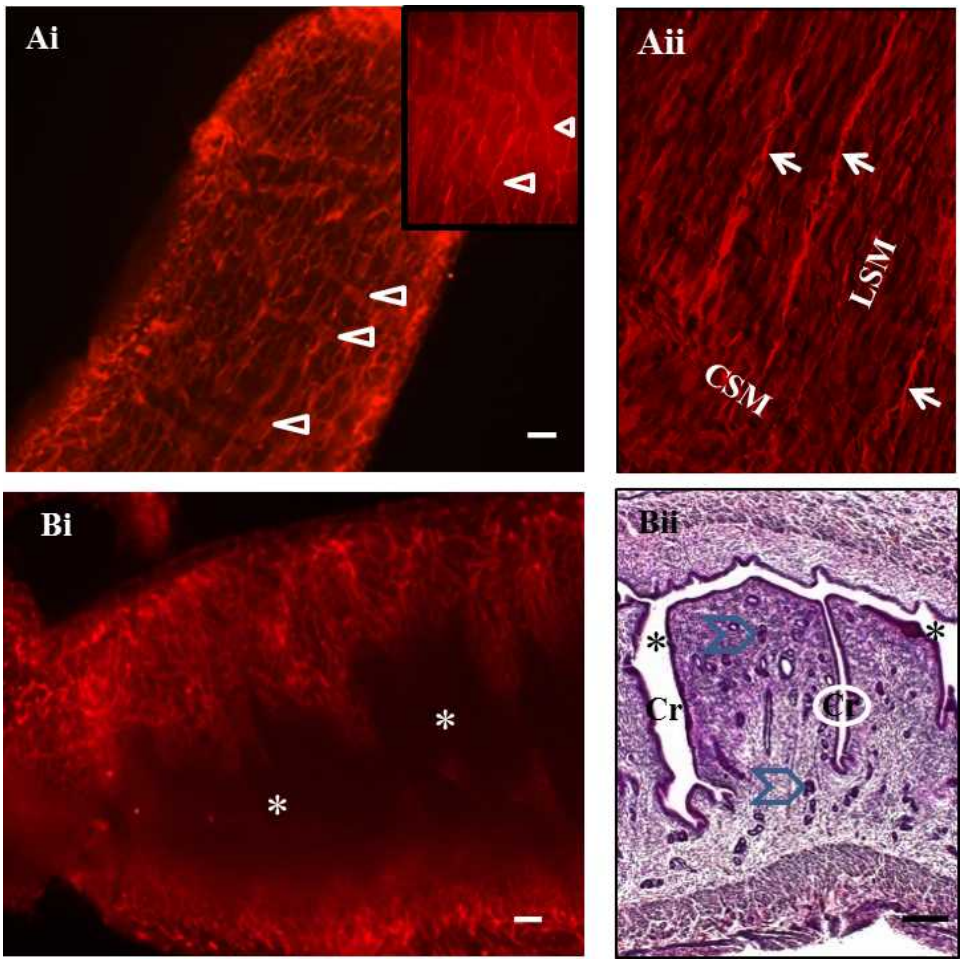

FIG. 2. Photomicrographs of the external serosal and internal mucosal surfaces of a diestrous, virgin B6 uterus. The mesentery supporting the uterus and providing its blood supply (mesometrium) is uppermost in all images. In whole-mount images (**Ai** and **Bi**), $CD31^+$ cells are red. Whole-mount staining in **Ai** shows the external surface of the uterus (serosa). Superficial vessels were narrow and appeared to be aligned with the outer longitudinal smooth muscle layer of the uterine wall. An image of a paraffin section from a diestrous uterus (**Aii**) confirms parallel vessel alignment (arrows) with the outer longitudinal smooth muscle layer (LSM) in an H&E-stained, red pseudocolored section. This vascular relationship terminated at the inner circular smooth muscle (CSM) layer. On the serosal side, deeper, wider, blunt-ended $CD31^+$ structures were seen (arrowheads) that had the typical appearance of lymphatics (higher-power inset in **Ai**). In other whole-mount specimens, lymphatic identity of these vessels was confirmed using LYVE-1 staining (data not shown). An image (**Bi**) illustrates vessels of the undulating virgin uterine mucosa exposed by a midsagittal cut. The uterine lumen (*) is dark and lies between the vascularized walls. Also shown (**Bii**) is an H&E section of a similarly cut virgin uterus showing the uterine lumen (*), lined by epithelium; deep folds called crypts (Cr) and uterine glands that branch from the crypt bases (blue chevrons). During implantation, hatched blastocysts locate into antimesometrial crypts. Original magnification ×658 (**Aii**); bar = 200 μm (**Ai** and **Bi**) and 150 μm (**Bii**).

tation chamber were vividly $CD31^+$ on GD 5.5 (data not shown). This intense, positionally restricted reactivity, not present at GD 5.0, was sustained at GD 6.5 (Fig. 4, Ci, Ciii, and Civ) and at GD 7.5 (Fig. 5, D, Ei, and Eii) and extended to include the residual uterine lumen after GD 5.5. The initial superbright $CD31^+$ staining at GD 5.5 was on epithelial or endothelial cells, because $CD45^+CD31^+$ cells were infrequent (<1%) in whole mounts at this time. At GD 6.5 and GD 7.5, approximately 50% of $CD45^+$ cells examined by whole-mount immunostaining expressed visually detectable CD31 (Supplementary Fig. S2B). FACS analyses performed at GD 7.5 and GD 9.5 confirmed $CD45^+$ cells coexpress CD31 (Supplementary Fig. S2, C and D).

At GD 5.5, angiogenesis involving web formation became prominent. Broad vascular webs continued to be seen until midpregnancy, when the present study concluded. Web-type angiogenesis (encircled areas in Fig. 4Cii, illustrating GD 6.5) was most prominent in the $CD45^+$ cell-enriched decidua basalis (Fig. 4Cii) and in lateral decidua (asterisk in Fig. 4Ciii, illustrating GD 6.5), a region relatively deficient in $CD45^+$ cells. In decidua basalis, webbed vessels, estimated to have a mean lumen width of 8.6 ± 3.1 μm, were relatively short, densely packed, and present at varying depths. Webbed vessels of lateral decidua were narrower (4.5 ± 1.2 μm, $P < 0.001$), less complex, and less densely stacked than in decidua basalis. Neither region showing prominent webbed angiogenesis contained GFP^+ trophoblast cells at GD 5.5 or GD 6.5. Sprouting angiogenesis appeared to be more prevalent than webbed angiogenesis antimesometrially (Fig. 4Civ, illustrating GD 6.5). Antimesometrial vessels were found in zones that appeared to represent the early primary decidua closer to the conceptus and the later developing secondary decidua closer to the uterine wall (Fig. 4Civ, illustrating GD 6.5). Vessels of the primary decidual zone were wider in lumen diameter (6.8 ± 1.6 μm) and had an average of 10.7 branch points per grid quadrant. Vessels in the secondary decidual zone were narrower (3.7 ± 0.7 μm, $P < 0.001$) and more highly branched (average of 19.5 points per quadrant, $P < 0.05$). By GD 7.5, antimesometrial angiogenesis was less evident, and vessels appeared to be more mature (pruned). Whole-mount

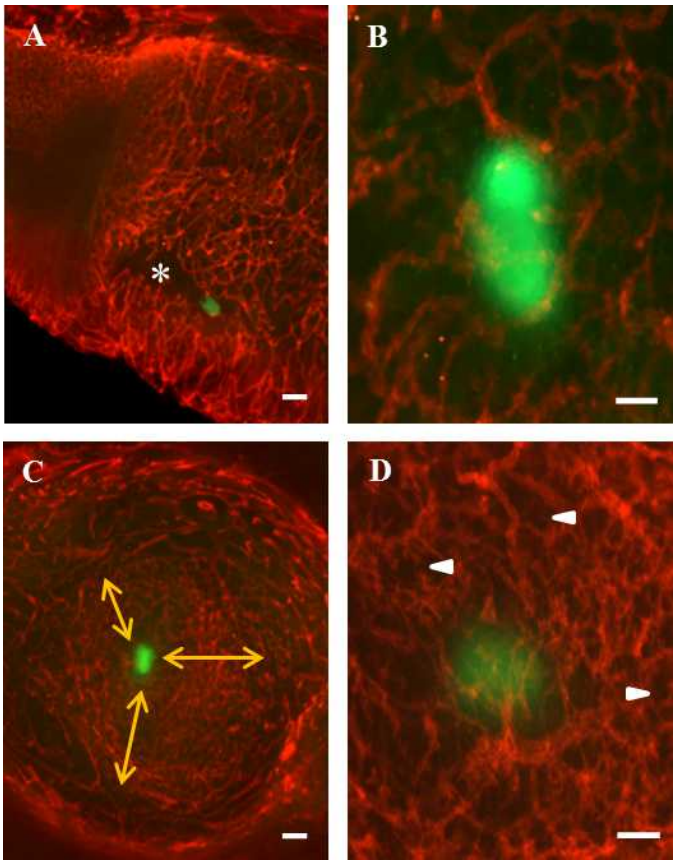

FIG. 3. Photomicrographs of whole-mount GD 4.5 and GD 5.0 uteri containing $Gfp^{+/-}$ (green) conceptuses and stained with PE-CD31 (red). **A**) Sagittally cut uterus with the mesometrial aspect to the top of the image. The green conceptus has implanted antimesometrially within a crypt (*). The walls of the crypt are closing around the conceptus (compare regions marked by * to Fig. 2Bi). **B**) Angiogenesis is not evident at GD 4.5. **C**) Transverse cut at the implanting conceptus on GD 5.0. Note the lateral decidual vessels with the view extending towards the antimesometrial region. Angiogenesis (sprouting tip cells), widespread around the conceptus, radiates in all directions (three arrows) but does not yet involve the deep mucosal vessels. **D**) Angiogenesis is reflected by the increased number of vessels and by the reduced vascular detail when compared to **B**. Arrowheads indicate sprouting angiogenesis. Bar = 200 μm (**A** and **C**) and 100 μm (**B** and **D**).

analyses between GD 5.5 and GD 7.5 provided more resolution of angiogenesis and greater detail concerning decidual vascular heterogeneity than standard histological sections (compare Fig. 4, A and Ci–iv).

Movement of individual trophoblast cells away from conceptuses was first detected at GD 6.5 whether conceptuses were heterozygous or homozygous for *Gfp* (heterozygous, see Fig. 5; homozygous, see Supplementary Fig. S1B). The initial advancement of trophoblasts into decidua basalis was as small, round, single cells that lay between vessels (i.e., merged images lacked yellow coloration) (Fig. 5, A, Ci, and Cii, and Supplementary Fig. S1B). No enrichment was found in $CD45^+$ cells at sites containing the initially invading $Gfp^{+/-}$ trophoblast cells (Fig. 5, Ci and Cii). Trophoblast advancement was robust not only from the ectoplacental cone into the decidua basalis but also at the opposite embryonic pole (Fig. 5, Ei and Eii). Fewer trophoblasts advanced laterally (Fig. 5, D and Ei), and these traveled shorter distances (372 μm in Fig. 5D) than trophoblasts moving out from the embryonic poles (1498 μm mesometrially and 1192 μm antimesometrially in the implant sites illustrated in Fig. 5, D and Eii). By GD 7.5, invading trophoblasts had become more heterogeneous in size (Fig. 5, Ci, Cii, D, Ei, and Eii).

At GD 6.5 and GD 7.5, leukocytes, many of which expressed CD31 (Supplementary Fig. S2, B–D), associated with vessels of decidua basalis (Fig. 5Cii). These $CD45^+$ cells were of multiple lineages and many were not $NK1.1^+$ uNK cells (compare Supplementary Figs. S2F and S2E). Additionally, irregularly shaped, $CD45^+$ cells were prominent in antimesometrial decidua (Fig. 5B). Upon careful study, these irregularly shaped cells (negative in whole-mount staining for F4/80, Gr-1, and CD11c, but positive for CD11b; not shown) were also identified mesometrially in the leukocyte-dense area and in the lateral decidua. Indeed, these immature, monocyte-like cells appeared to be uniformly distributed across the entire decidua as single cells and were never observed in conjugates or clusters with other $CD45^+$ cells or with trophoblasts. One third of the irregularly shaped $CD45^+$ cells expressed class II major histocompatibility complex (MHC; data not shown), suggestive of antigen presentation capability, but none expressed detectable CD31 in whole-mount staining (data not shown).

Gestational Days 8.5 and 9.5. At GD 8.5 and GD 9.5, mouse fetuses show rapid development and growth, including head folding, continuing somite differentiation, organogenesis, and outgrowth of the allantois, which will fuse with the chorionic plate and complete placental differentiation during GD 9 [26]. Over this interval, antimesometrial decidua regresses, and leukocytes increase in number in decidua basalis [8, 27, 28]. Whole-mount staining of GD 8.5 implant sites showed these plus additional features. Intensity of CD31 staining around conceptuses decreased, apparently due to disruption of the vivid $CD31^+$ region by radial, extravascular trophoblast outgrowth and amniotic cavity enlargement (Fig. 6A). Vessels were less densely packed immediately surrounding the conceptus than at earlier times due to expansion of the fluid-filled fetal amniotic cavity (compare Figs. 6A and 3C). Antimesometrial trophoblast expansion consumed space previously occupied by the antimesometrial decidua and its vessels. Connectivity of antimesometrial vessels was reduced (compare Figs. 6B and 4Civ). Web-type angiogenesis continued in lateral and basal deciduas (Fig. 6, C and D), but no vessels resembling spiral arterioles were observed. Leukocytes, including numerous $CD45^+CD31^+$ leukocytes, were more abundant in the distal, densely vascular decidual basalis (Fig. 6, C and D) than in decidua basalis proximal to the trophoblast interface (data not shown). At GD 8.5, many large and small $CD45^+$cells showed irregular shapes (pseudopodia suggesting activation and/or movement) (see asterisk in Fig. 6D), and leukocyte-leukocyte (see plus symbol in Fig. 6D), but not leukocyte-trophoblast, conjugates were commonly observed. $CD45^+$ cell conjugation and shape alteration occurred distal to (Fig. 6D) as well as proximal to (data not shown) trophoblast. Occasionally, clusters of more than two leukocytes were seen (data not shown).

At GD 9.5, webbed angiogenesis continued mesometrially (Fig. 7A) in the presence of high numbers of $CD31^+$ leukocytes (Fig. 7B). By this time, migrating trophoblast cells had reached the region enriched in $CD45^+$ cells (Fig. 7C), and very large cells contributed to trophoblast heterogeneity (Fig. 7D). Many trophoblast cells had now established an intimate relationship with endothelium in vessels at the decidual-conceptus interface (Fig. 7D). Yellow in merged images represents colocalized trophoblasts and endothelial cells, and these images suggested neither displacement nor damage of endothelial cells during trophoblast entry into vessels. Trans-endothelial trophoblast migration was apparent at some sites

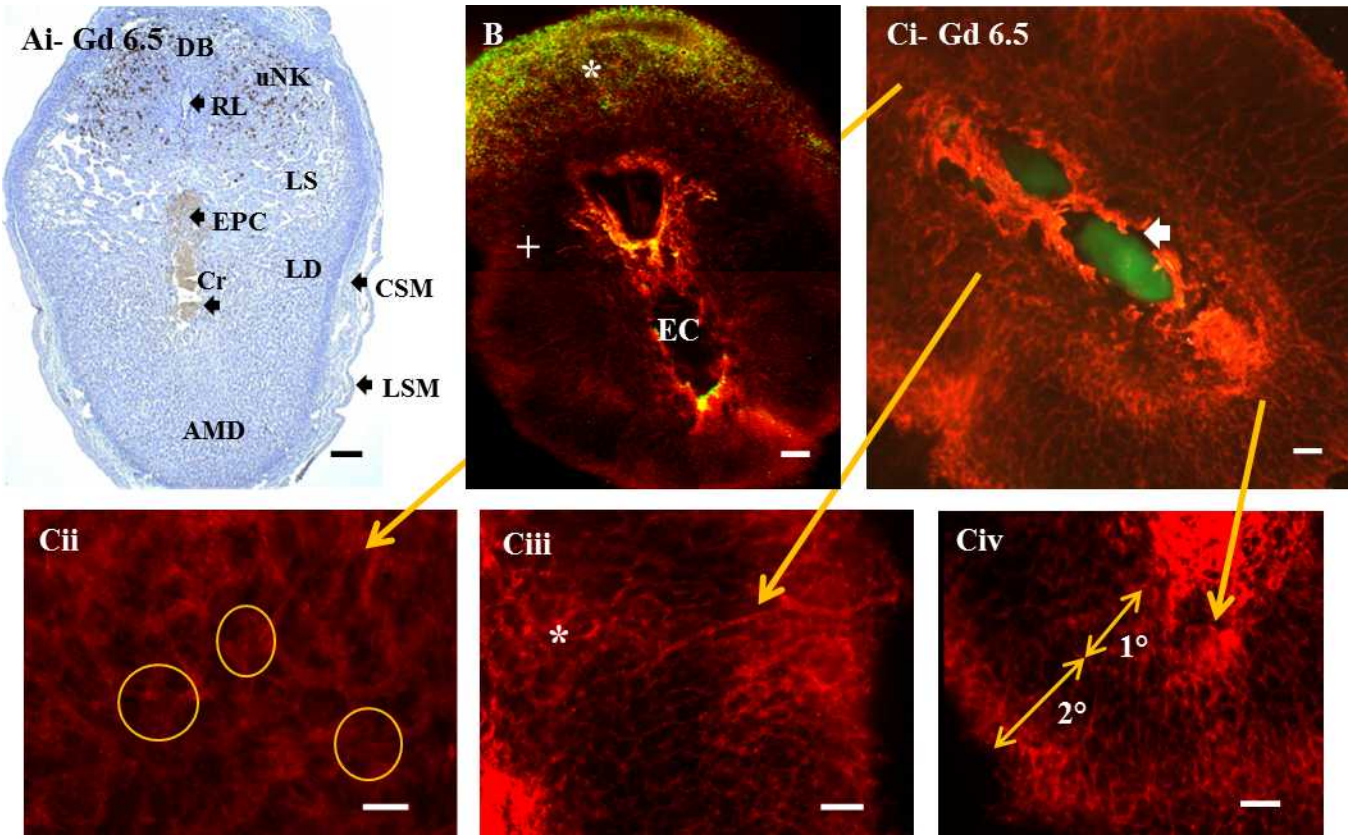

FIG. 4. Gestational Day (labeled as Gd) 6.5 B6 uteri containing primitive streak-stage embryos. Mesentery supporting the uterus and providing its blood supply (mesometrium) is uppermost. **A**) DBA lectin-stained paraffin section reveals uNK cells (brown) in decidua basalis. Some endothelial cells are also DBA^+. The central primitive-streak embryo, its extraembryonic region, and ectoplacental cone (placental primordium [EPC]) are visible in the embryonic crypt (Cr) below the residual uterine lumen (RL), which will close as pregnancy proceeds. Large lateral decidual sinusoids (LS) are developing. **B**) In the GD 6.5 whole-mount image of a normal B6 conceptus, $CD45^+$ cells are pseudocolored green, and $CD31^+$ cells are pseudocolored red. The $CD45^+$ cells appear as a dense cloud (*) with a crescent shape along the base of the decidua basalis (myometrium was removed in this specimen, originally photographed in black and white). $CD45^+$ cells occur but are not enriched in decidua basalis proximal to the implantation chamber (EC) or in lateral decidua (+). **C**) In PE-CD31-stained whole-mount image C with a $Cfp^{+/-}$ conceptus, $CD31^+$ cells are red, and conceptus-derived cells are green. **Ci**) Low-power, whole-mount image from the same gestational time as images in **A** and **B** with EPC uppermost and primitive-streak embryo below. An arrow marks the embryonic crypt surrounded by superbright $CD31^+$ cells. At GD 5.5, intense CD31 reactivity surrounded conceptuses but did not extend to the residual uterine lumen (data not shown). By GD 6.5, the superbright $CD31^+$ staining had extended to include the residual uterine lumen (not shown; located outside of the image above the $Cfp^{+/-}$ conceptus). Control staining (data not shown) was used to verify that neither non-specific antibody binding nor autofluorescence contributed to the $CD31^+$ or $CD45^+$ decidual staining patterns. **Cii**–**Civ**) Typical regional vascular differences shown at higher magnification. In **Cii**, decidua basalis, the most densely vascular region, is shown. Here, the poorly defined, diffuse, actively angiogenic vessels (examples encircled) are associated with high numbers of $CD45^+$ cells that, from GD 6.5, could coexpress CD31 (not shown). Conjugated $CD45^+$ cells remained rare (not shown). In **Ciii**, which shows lateral decidua (LD), angiogenesis differed by proximity to the implantation crypt. Webbed angiogenesis was more prominent proximal to the crypt (medially, marked by *), and sprouting angiogenesis was more prominent laterally, where very long, unbranched vessels were also seen (termination of arrow). In **Civ**, antimesometrially, vessels of the primary decidua (1°; proximal to the conceptus) differed from those of secondary decidua (2°; closer to the uterine wall). AMD, antimesometrial decidua; CSM, inner circular smooth muscle of uterine wall; LSM, outer longitudinal smooth muscle of uterine wall. Bar = 150 μm (**A**), 200 μm (**B** and **Ci**), and 100 μm (**Cii**–**Civ**).

(arrows in Fig. 7D). Unexpectedly, trophoblast appeared to occlude the lumens of some arterioles (trophoblast does not have venous associations). As marked by arrowheads in Fig. 7D, a series of closely related, occluded vessels occurred. Such sets of rings may represent cross-sections of spiral vessels. In Figure 7A, a large, remodeling vessel acquiring a spiral shape (arrows) was also present, distal to the region of the partial/complete trophoblast plugs. Trophoblastic plugs are transient structures observed during human, baboon, and macaque spiral arterial remodeling [29, 30].

DISCUSSION

Many techniques have been used to address lymphocyte functions and trophoblast-endothelial cell interactions in mouse and human pregnancies [31]. Combined application of flow cytometric analyses and whole-mount immunostaining to investigate early mouse implant site decidua confirmed, integrated, and enlarged previous knowledge. New insights were gained by simultaneous focus on three cell types: leukocytes, trophoblasts, and endothelium. Flow cytometric analyses of $CD45^+$ cells in whole decidua indicated fluctuations in proportions of several leukocyte populations such as uNK cells, immature monocytes, and B cells but relative stability in the proportions of others, such as granulocytes, DCs, and T cells. The uNK cells were defined as $CD3^-NK1.1^+$, a phenotype of uNK cells that declines between implantation and midpregnancy [32, 33]. The DBA lectin that defines the expanding uNK cell subset was not successful as a fluorochrome-tagged reagent in whole-mount staining (data not shown). This, plus presentation of the data as a proportional analysis of uNK cells against all decidual $CD45^+$ cells rather than as absolute uNK cell numbers in only the decidua basalis

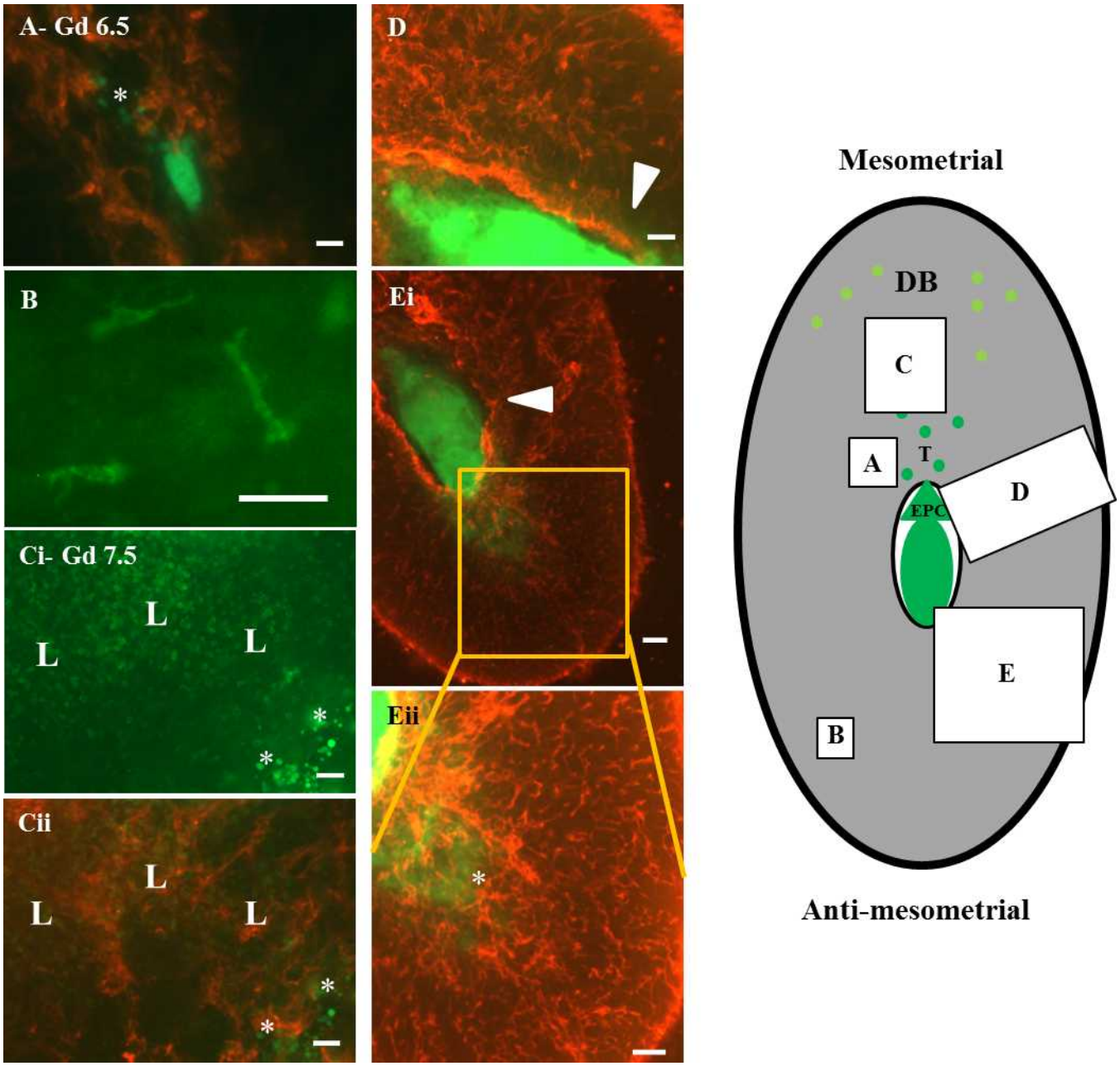

FIG. 5. Whole-mount staining of GD 6.5 (labeled as Gd; **A** and **B**) and GD 7.5 (**C**–**E**) B6 implant sites. Mesentery supporting the uterus and providing its blood supply (mesometrium) is uppermost. $CD31^+$ cells are red, and $CD45^+$ cells are green, as are conceptus-derived GFP-expressing cells, which are a distinct, more intense, and diffuse yellow-green. Diagram to the right localizes the general positions of the whole-mount images within the decidualized (gray) implant site. Cells of conceptus origin are darker green with ectoplacental cone (EPC) and migrating trophoblasts (T) shown schematically. Yellow-green circles represent $CD45^+$ cells enriched in decidua basalis. By GD 6.5, all B6 conceptuses had given off individual migrating trophoblast cells predominantly into decidua basalis (star in **A**). At GD 6.5 and GD 7.5, CD31 staining around the embryonic crypt was vivid (**D**, **Ei**, and **Eii**). At GD 7.5 (**Ci**, **Cii**, **D**, **Ei**, and **Eii**), trophoblast migration was obvious in all directions. In **Ci**, mesometrial invading trophoblasts (*) are shown with $CD45^+$ cells (L) in a green channel image. No enrichment of $CD45^+$ cells is apparent at the trophoblast interface. In **Cii**, the same field is shown merged with the red channel image revealing the greater relationships of $CD45^+$ cells with decidual vessels than with trophoblasts. Trophoblasts also at this stage were not interacting with endothelial cells (i.e., yellow is absent from the merged image). In **D** and **Ei**, implant sites from different litters, lateral trophoblast invasion towards the region of vascular sinus development is shown (arrowheads), whereas in **Eii**, a higher power image of **Ei**, antimesometrial invasion is shown (*). Many trophoblasts at the embryonic poles now appeared as contiguous cell sheets. Unusually shaped $CD45^+$ "stellate" cells were prominent in lateral and antimesometrial decidua (green in **B**, a high power image of a region with no invading trophoblasts), but they were generally masked mesometrially by the high numbers of other $CD45^+$ cells. Some "stellate" cells (~30%) reacted with monoclonal antibody to mouse class II MHC antigen (data not shown). In comparison with vessels of decidua basalis (**C**), vessels of the antimesometrial decidua (**Eii**) were shorter, narrower, had less webbing, and did not radiate from a single point. Mesometrial vessels were wider, longer, linked with a loop pattern, and converged on a CD31 superbright region suspected to be the residual uterine lumen. These decidual vascular differences were established before significant trophoblast invasion. Bar = 100 μm (**A**, **Ci**, and **Cii**) 50 μm (**B**), 150 μm (**D** and **Eii**), and 200 μm (**Ei**).

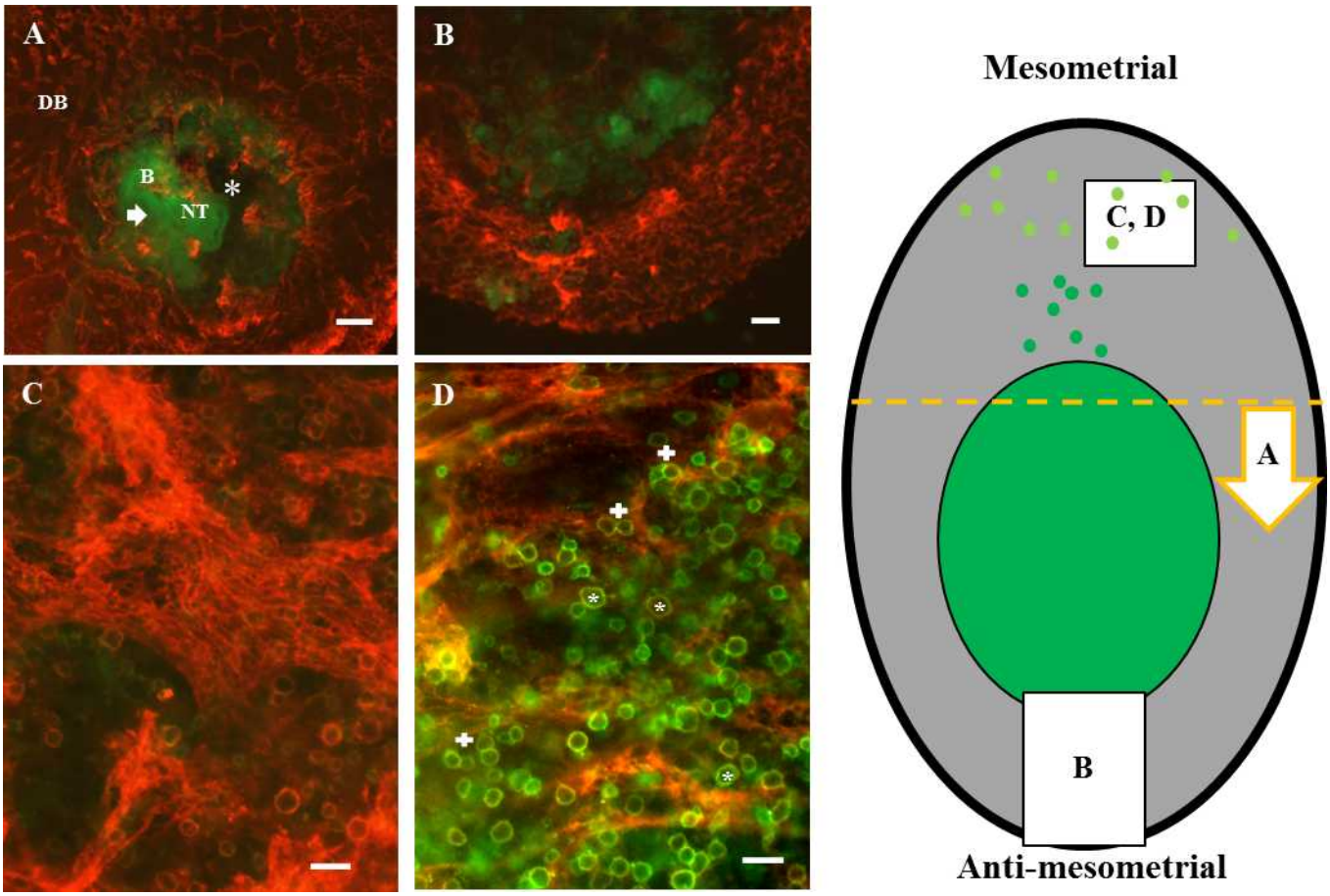

FIG. 6. Whole-mount staining of GD 8.5 B6 implant sites. $CD31^+$ cells are red, $CD45^+$ cells are green, and $CD45^+CD31^+$ cells are orange-yellow. Green of GFP-expressing cells was distinct from $FITC^+$ cells. The diagram to the right localizes the general positions of the whole-mount images within the decidualized (gray) implant site. Darker green represents the conceptus-occupied area and mesometrially migrating trophoblasts. Yellow-green circles represent $CD45^+$ cells enriched in decidua basalis. The yellow dashed line represents the cut made to provide specimen (**A**); the arrow shows the orientation of the observer viewing the image in **A**, a transverse section viewed towards the anti-mesometrial side. **A**) The open neural tube (NT) of the fetus. Its curved body (B) and tail are visible, as is the amniotic cavity (*). Radial growth of trophoblast, largely as a cell sheet, is seen into regions that had previously displayed strong CD31 expression (arrowhead)**.** The implant site is strongly indented by maternal vessels. In the remaining panels, mesometrium is uppermost. **B** shows outward-growing antimesometrial trophoblast and the thinning decidual region, where vessels no longer appear angiogenic but mature (pruned) or with diminished connections (regressing). At GD 8.5, trophoblasts still showed no interactions with endothelial cells. **C** and **D**) Implant sites from different litters. $CD45^+CD31^+$ leukocyte enrichment of decidua basalis (DB) is illustrated. In **C**, note a wide vessel displaying webbed angiogenesis. Trophoblast cells were not present in this region. In **D**, note the widespread changes in $CD45^+$ cell shape apparent at GD 8.5 (*). These changes include extension of processes suggestive of activation and/or mobilization and conjugation between pairs of $CD45^+$ cells (+). $CD45^+$ cell-trophoblast conjugates were not observed. Bar = 500 μm (**A** and **B**) and 50 μm (**C** and **D**).

or the mesometrial lymphoid aggregate of pregnancy explains the apparent discordance of the present data with those of earlier quantitative studies. Figure 1A and Supplementary Figure S2, E and F, emphasize that comprehensive understanding of leukocyte biology in early decidua has not been achieved.

Although NK cells and T cells expressed activation markers from GD 4.5, morphologic evidence for activation (leukocyte conjugate formation and for migration suggested by shape changes) was uncommon before GD 8.5, which is 4–5 days after blastocyst hatching and, thus, a time consistent with primary immune responses to antigens exposed at hatching. It is also the GD at which human indicator blood lymphocytes used in assays of adhesion to mouse decidual substrates first recognize changes in mouse decidual T cells and conjugate with them [34]. The most highly activated cells ($CD69^+$) in early decidua appear to be uNK cells, as reported in older lytic function assays [35]. However, assays under more supportive culture conditions (i.e., interleukin 15 and stroma) are needed to precisely define levels of uNK cell functions, because uNK cells also had the highest regulatory molecule (KLRG1) expression and this varied by GD. The proportions of decidual T cells observed in the present study are lower than those reported by others. Of note, most other reports addressed time points later than the morphologically suggested, GD 8.5 activation of $CD45^+$ cells. The possibility that any of the analyzed leukocytes are fetal in origin is excluded, because the aorta/gonad/mesonephros region where fetal hematopoietic stem cells first differentiate is not present before GD 8.5. GD 10.5 is the first day of detectable pre-B cell development [36], and GD 11.5 is the first day the thymus becomes populated [37]. Studies were not conducted after GD 9.5, because thickness of the placenta prevented proper antibody penetration, success in coverslip mounting, and adequate tissue illumination. A notable difference between early murine and human deciduas is the much higher level of B cells in mice (~5%–25%) versus reports of no [38] or rare [39] B cells in humans. The gain in abundance of immature monocyte-like cells during decidual development has not been previously reported. These CD31-low, $F4/80^-$, $CD11c^-$, $Gr\text{-}1^-$, $CD11b^+$,

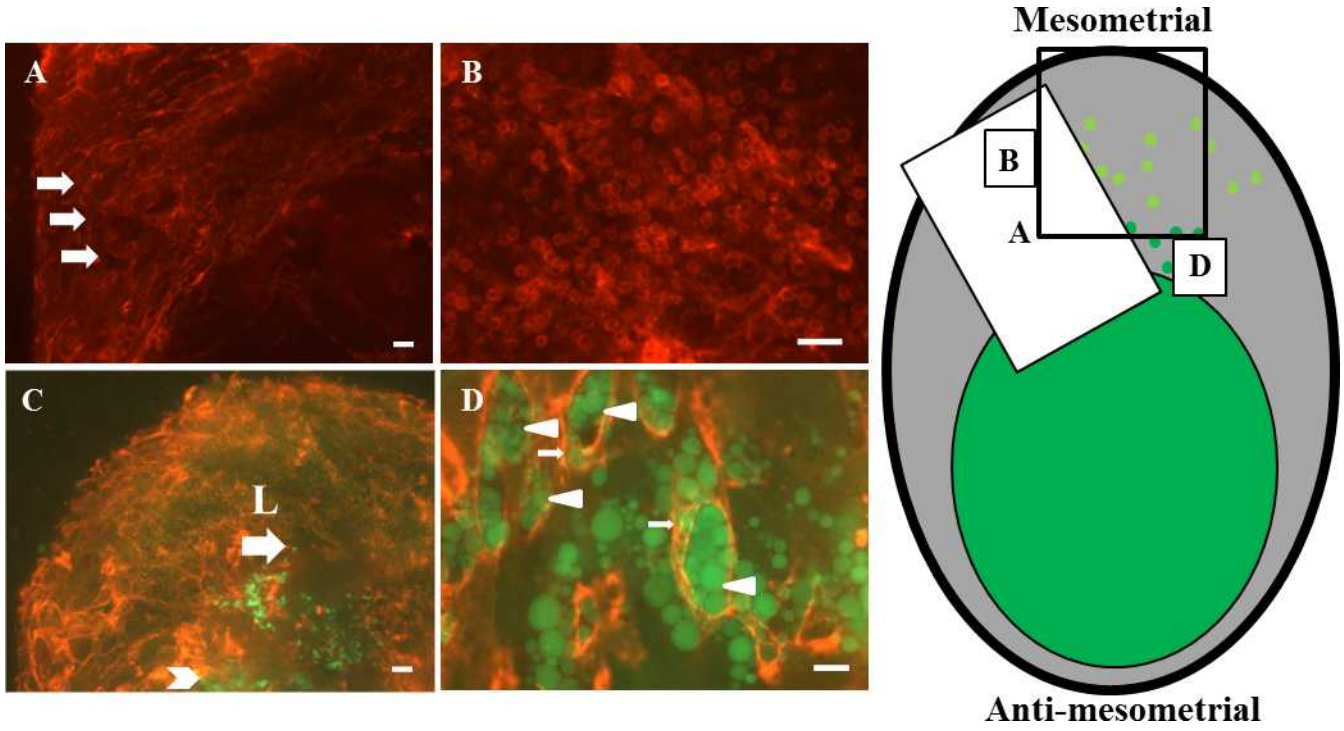

FIG. 7. Whole-mount staining of GD 9.5 B6 implant sites showing CD31 (red) alone (**A** and **B**) or CD31 (red) merged with CD45 (green) and GFP-expressing trophoblasts that are brighter green (**C** and **D**). Diagram to the right localizes the general positions of the whole-mount images in the decidualized (gray) implant site. Darker green represents the conceptus-occupied area and mesometrially migrating trophoblasts. Yellow-green circles represent $CD45^+$ cells enriched in decidua basalis. The black rectangle represents the position of the image in **C**. **A**) Mesometrial angiogenesis continued at GD 9.5, as indicated by the prominence of webbed vessels. **B**) $CD31^+$ leukocytes remained abundant in this angiogenic region. **C** and **D**) In merge images of decidua basalis, more deeply invaded trophoblasts appeared as single cells (arrow) that were reaching the leukocyte "cloud" (L). Trophoblasts closer to the fetus were more tissue-like (arrowhead in **C**). At higher power (**D**), trophoblasts of a wide variety of sizes now interacted with endothelium (arrowheads in **D**), including transendothelial migration (arrows in **D**). Many vessel lumens appeared to be occluded or partly occluded by trophoblasts, and the occluded structures appeared to be coils of a spiral vessel. In lower-power images of decidua basalis (**A**), larger vessels within areas of active angiogenesis seemed to be acquiring a spiral appearance (arrows in **A**). Bar = 200 μm (**A** and **C**), 100 μm (**B**), and 50 μm (**D**).

$CD45^+$ immune cells could be further divided into two populations that either expressed MHC class II (~30% of the total population examined by flow cytometry), characteristic of antigen-presenting cells, or lacked the expression of this molecule. Whole-mount analysis of this unusual cell subset showed uniform distribution across the entire decidua, suggesting functions quite distinct from the leukocytes enriched in decidua basalis.

Many round, $CD45^+$ cells in decidua basalis acquired strong expression of CD31 at GD 6.5, suggesting changes involving uNK cells. CD31 expression by lymphocytes is well known. In humans, some first-trimester $CD3^-CD56^+$ uNK cells are $CD31^+$ [40], and in blood NK cells, cross-linkage of CD31 triggers cytoskeletal rearrangement [41]. CD31 is also thought to differentiate naïve ($CD31^+$) from activated ($CD31^-$) T cells [42]. More recently, human $CD31^+$, but not $CD31^-$, T cells or NK cells were reported as angiogenic cells contributing to endothelial repair, migrating in response to VEGFA and CXCL12 (signals also important in recruitment of endothelial progenitor cells) and secreting angiogenic cytokines [43]. Mice homozygous for CD31 deletion are normally fertile to at least 6 mo of age and have no apparent defects in angiogenesis or transendothelial leukocyte migration [44]. No analyses of early implant sites of CD31-null mice have been reported. The elevated expression of CD31 around the embryonic crypt on GD 6.5 and GD 7.5, with decline at GD 8.5, was previously reported [45, 46]. Those studies concluded that the CD31 staining was not over endothelial cells and postulated that leukocytes or dying epithelial cells were stained [46]. Our GD 5.5 data exclude leukocytes as the source of the superbright CD31 signal and suggest a stromal region that may separate leukocytes from early invading trophoblasts (Fig. 5C). Other genes and molecules are coincidently upregulated in peri-implant site stroma, including *Cox2* [45], *Wnt* family members [47], and other progesterone-regulated genes [48]. Decline in CD31 expression around the embryonic crypt from GD 8.5 appeared to be due to physical disruption/displacement of $CD31^+$ cells due to radial trophoblast outgrowth. Trophoblast phagocytosis [49] of epithelial and decidual cells surrounding the embryonic crypt also likely contributed to the decline in CD31 superbright stromal cells.

Angiogenesis, as evidenced by widespread appearance of endothelial tip cells (Fig. 3D), accompanied implantation at GD 5.0. VEGF and FLK1 (VEGFR2) heavily influence sprout frequency and directionality [50]. VEGFA expression becomes widespread immediately around the blastocyst at GD 5.0, then spreads mesometrially and antimesometrially at GD 6–8 [51]. In other models, induction of endothelial tip cells additionally requires Delta-like ligand-1 (DLL1) from sources exogenous to endothelial cells [52]. It will be important to determine if the paradigm of DLL1 induction of tip cells applies to implant site angiogenesis, both to identify the cells providing the exogenous signaling and to determine whether trophoblasts and/or ovarian hormones regulate DLL1. Fusion of sprouts is an essential step in vessel formation. During embryonic development, macrophages often bridge the connection between a spouting cell and its fusion target [53]. This maybe

the role of the immature monocyte-like $CD11b^+$ cells found throughout decidua.

Other methods of new vessel formation include vasculogenesis, intussusception, and flow-driven remodeling [54]. The complexity of implant site vessels, illuminated by whole-mount staining, suggests multiple mechanisms contribute to decidual neovessels. The web-like vessels may suggest intussusceptions, which define vascular formation and remodeling processes that combine two or more existing vessels. Intussusceptions also indicate primitive vascular networks arising by vasculogenesis in which vessel formation involves circulating endothelial progenitor cells. Webbed angiogenesis was prominent in lateral decidual regions that would become vascular sinuses and in the more densely vascular decidua basalis. Because only the latter region is leukocyte enriched, induction of this type of angiogenesis appears to be independent of leukocyte functions. More probably, leukocytes, particularly those expressing CD31, may promote the abundance, rather than affect the nature, of neovessels.

Use of *Gfp*/*Gfp* studs provided conceptuses with tagged trophoblast. This permitted visualization of the very earliest steps in trophoblast migration undertaken by single, detached, ''pioneering'' cells. These single-cell migrations were not associated with either endothelium or leukocytes, and conjugates between trophoblasts and $CD45^+$ cells were never seen. Rather, trophoblasts from the ectoplacental cone migrated towards the leukocyte-enriched decidua basalis, whereas trophoblast outgrowth in other directions was independent of a leukocyte-enriched target region. At GD 9.5, some trophoblasts became intravascular. Unexpectedly, they appeared to occlude some decidual vessels, a finding that parallels trophoblastic plugs of spiral arterioles in humans [30]. Dispersion of human trophoblastic plugs opens the intervillous space to maternal blood flow. In mice, trophoblast plugs may transition hemodynamic control from the mother to conceptus, because it occurs at the time the gestationally induced decline in maternal blood pressure is reversed [55].

In summary, application of whole-mount staining to early mouse implant sites containing $Gfp^{+/-}$ conceptuses is successful. It images living, intact decidua in greater detail than histological sections, vascular casting, or ultrasound studies. The simplicity and speed of this technique suggest it will have wide application for studies of pregnancy in genetically modified or experimentally manipulated mice. Cell surface reagents successful in flow cytometric analyses usually work very well in whole-mount staining, enabling a wide scope of experimental questions. In other tissues, confocal microscopy and cell permeabilization protocols successfully reveal even greater cellular detail and merit development for early mouse decidua [52].

ACKNOWLEDGMENT

We thank Dr. Shawn P. Murphy, University of Rochester, for helpful suggestions and extended discussions and Ms. Joanne H. Lim, Ms. Allison Felker, and Mr. Matthew Rätsep for technical assistance.

REFERENCES

1. Abrahamsohn PA, Zorn TM. Implantation and decidualization in rodents. J Exp Zool 1993; 266:603–628.
2. Altmae S, Martinez-Conejero JA, Salumets A, Simon C, Horcajadas JA, Stavreus-Evers A. Endometrial gene expression analysis at the time of embryo implantation in women with unexplained infertility. Mol Hum Reprod 2010; 16:178–187.
3. Welsh AO, Enders AC. Chorioallantoic placenta formation in the rat: II. Angiogenesis and maternal blood circulation in the mesometrial region of the implantation chamber prior to placenta formation. Am J Anat 1991; 192:347–365.
4. Maynard S, Epstein FH, Karumanchi SA. Preeclampsia and angiogenic imbalance. Annu Rev Med 2008; 59:61–78.
5. Quenby S, Nik H, Innes B, Lash G, Turner M, Drury J, Bulmer J. Uterine natural killer cells and angiogenesis in recurrent reproductive failure. Hum Reprod 2009; 24:45–54.
6. Tidwell SC, Ho HN, Chiu WH, Torry RJ, Torry DS. Low maternal serum levels of placenta growth factor as an antecedent of clinical preeclampsia. Am J Obstet Gynecol 2001; 184:1267–1272.
7. Burton GJ, Jauniaux E, Charnock-Jones DS. The influence of the intrauterine environment on human placental development. Int J Dev Biol 2010; 54:303–312.
8. Croy BA, van den Heuvel MJ, Borzychowski AM, Tayade C. Uterine natural killer cells: a specialized differentiation regulated by ovarian hormones. Immunol Rev 2006; 214:161–185.
9. Li XF, Charnock-Jones DS, Zhang E, Hiby S, Malik S, Day K, Licence D, Bowen JM, Gardner L, King A, Loke YW, Smith SK. Angiogenic growth factor messenger ribonucleic acids in uterine natural killer cells. J Clin Endocrinol Metab 2001; 86:1823–1834.
10. Li C, Houser BL, Nicotra ML, Strominger JL. HLA-G homodimer-induced cytokine secretion through HLA-G receptors on human decidual macrophages and natural killer cells. Proc Natl Acad Sci U S A 2009; 106: 5767–5772.
11. Blois SM, Klapp BF, Barrientos G. Decidualization and angiogenesis in early pregnancy: unravelling the functions of DC and NK cells. J Reprod Immunol 2011; 88:86–92.
12. Demir R, Kayisli UA, Cayli S, Huppertz B. Sequential steps during vasculogenesis and angiogenesis in the very early human placenta. Placenta 2006; 27:535–539.
13. Wang C, Tanaka T, Nakamura H, Umesaki N, Hirai K, Ishiko O, Ogita S, Kaneda K. Granulated metrial gland cells in the murine uterus: localization, kinetics, and the functional role in angiogenesis during pregnancy. Microsc Res Tech 2003; 60:420–429.
14. Tayade C, Hilchie D, He H, Fang Y, Moons L, Carmeliet P, Foster RA, Croy BA. Genetic deletion of placenta growth factor in mice alters uterine NK cells. J Immunol 2007; 178:4267–4275.
15. Bouchentouf M, Forner KA, Cuerquis J, Michaud V, Zheng J, Paradis P, Schiffrin EL, Galipeau J. Induction of cardiac angiogenesis requires killer cell lectin-like receptor 1 and alpha4beta7 integrin expression by NK cells. J Immunol 2010; 185:7014–7025.
16. Pober JS. Immunobiology of human vascular endothelium. Immunol Res 1999; 19:225–232.
17. Sorensen EW, Gerber SA, Frelinger JG, Lord EM. IL-12 suppresses vascular endothelial growth factor receptor 3 expression on tumor vessels by two distinct IFN-gamma-dependent mechanisms. J Immunol 2010; 184:1858–1866.
18. Hibino N, Yi T, Duncan DR, Rathore A, Dean E, Naito Y, Dardik A, Kyriakides T, Madri J, Pober JS, Shinoka T, Breuer CK. A critical role for macrophages in neovessel formation and the development of stenosis in tissue-engineered vascular grafts. FASEB J 2011; 25:4253–4263.
19. Pitulescu ME, Schmidt I, Benedito R, Adams RH. Inducible gene targeting in the neonatal vasculature and analysis of retinal angiogenesis in mice. Nat Protoc 2010; 5:1518–1534.
20. Gerber SA, Moran JP, Frelinger JG, Frelinger JA, Fenton BM, Lord EM. Mechanism of IL-12 mediated alterations in tumour blood vessel morphology: analysis using whole-tissue mounts. Br J Cancer 2003; 88: 1453–1461.
21. Corson LB, Yamanaka Y, Lai KM, Rossant J. Spatial and temporal patterns of ERK signaling during mouse embryogenesis. Development 2003; 130:4527–4537.
22. Lugade AA, Sorensen EW, Gerber SA, Moran JP, Frelinger JG, Lord EM. Radiation-induced IFN-gamma production within the tumor microenvironment influences antitumor immunity. J Immunol 2008; 180: 3132–3139.
23. Croy BA, Zhang J, Tayade C, Colucci F, Yadi H, Yamada AT. Analysis of uterine natural killer cells in mice. Methods Mol Biol 2010; 612:465–503.
24. Zhang JQ, Biedermann B, Nitschke L, Crocker PR. The murine inhibitory receptor mSiglec-E is expressed broadly on cells of the innate immune system whereas mSiglec-F is restricted to eosinophils. Eur J Immunol 2004; 34:1175–1184.
25. Enders AC. Anatomical aspects of implantation. J Reprod Fertil Suppl 1976; 1–15.
26. Kaufmann MH. The Atlas of Mouse Development, rev. ed. London, U.K.: Elsevier Limited; 1992: 476–477.
27. Abrahamsohn PA. Ultrastructural study of the mouse antimesometrial decidua. Anat Embryol (Berl) 1983; 166:263–274.

28. Katz S, Abrahamsohn PA. Involution of the antimesometrial decidua in the mouse. An ultrastructural study. Anat Embryol (Berl) 1987; 176: 251–258.
29. Enders AC, King BF. Early stages of trophoblastic invasion of the maternal vascular system during implantation in the macaque and baboon. Am J Anat 1991; 192:329–346.
30. Pijnenborg R, Vercruysse L, Hanssens M. The uterine spiral arteries in human pregnancy: facts and controversies. Placenta 2006; 27:939–958.
31. Hatta K, MacLeod RJ, Gerber SA, Croy BA. Emerging themes in uterine natural killer cell heterogeneity and function. Am J Reprod Immunol 2012; 68:282–289.
32. Yadi H, Burke S, Madeja Z, Hemberger M, Moffett A, Colucci F. Unique receptor repertoire in mouse uterine NK cells. J Immunol 2008; 181: 6140–6147.
33. Chen Z, Zhang J, Hatta K, Lima PD, Yadi H, Colucci F, Yamada AT, Croy BA. DBA-lectin reactivity defines mouse uterine natural killer cell subsets with Biased gene expression. Biol Reprod 2012; 87(4):81, 1–9.
34. Hatta K, van den Heuvel MJ, Croy BA. NK cells detect changes in adaptive immunity within mouse decidua from gestation day eight. Placenta 2009; 30:501–506.
35. Gambel P, Croy BA, Moore WD, Hunziker RD, Wegmann TG, Rossant J. Characterization of immune effector cells present in early murine decidua. Cell Immunol 1985; 93:303–314.
36. de Andres B, Gonzalo P, Minguet S, Martinez-Marin JA, Soro PG, Marcos MA, Gaspar ML. The first 3 days of B-cell development in the mouse embryo. Blood 2002; 100:4074–4081.
37. Ikawa T, Masuda K, Lu M, Minato N, Katsura Y, Kawamoto H. Identification of the earliest prethymic T-cell progenitors in murine fetal blood. Blood 2004; 103:530–537.
38. Mincheva-Nilsson L, Baranov V, Yeung MM, Hammarstrom S, Hammarstrom ML. Immunomorphologic studies of human decidua-associated lymphoid cells in normal early pregnancy. Adv Exp Med Biol 1995; 371A:367–371.
39. Vince GS, Johnson PM. Leukocyte populations and cytokine regulation in human uteroplacental tissues. Biochem Soc Trans 2000; 28:191–195.
40. Marzusch K, Ruck P, Geiselhart A, Handgretinger R, Dietl JA, Kaiserling E, Horny HP, Vince G, Redman CW. Distribution of cell adhesion molecules on CD56++, CD3–, CD16– large granular lymphocytes and endothelial cells in first-trimester human decidua. Hum Reprod 1993; 8: 1203–1208.
41. Poggi A, Panzeri MC, Moretta L, Zocchi MR. CD31-triggered rearrangement of the actin cytoskeleton in human natural killer cells. Eur J Immunol 1996; 26:817–824.
42. Ashman LK, Aylett GW. Expression of CD31 epitopes on human lymphocytes: CD31 monoclonal antibodies differentiate between naive ($CD45RA^+$) and memory ($CD45RA^-$) CD4-positive T cells. Tissue Antigens 1991; 38:208–212.
43. Kushner EJ, MacEneaney OJ, Morgan RG, Van Engelenburg AM, Van Guilder GP, Desouza CA. $CD31^+$ T cells represent a functionally distinct vascular T cell phenotype. Blood Cells Mol Dis 2010; 44:74–78.
44. Duncan GS, Andrew DP, Takimoto H, Kaufman SA, Yoshida H, Spellberg J, de la Pompa JL, Elia A, Wakeham A, Karan-Tamir B, Muller WA, Senaldi G, et al. Genetic evidence for functional redundancy of platelet/endothelial cell adhesion molecule-1 (PECAM-1): CD31-deficient mice reveal PECAM-1-dependent and PECAM-1-independent functions. J Immunol 1999; 162:3022–3030.
45. Matsumoto H, Ma WG, Daikoku T, Zhao X, Paria BC, Das SK, Trzaskos JM, Dey SK. Cyclooxygenase-2 differentially directs uterine angiogenesis during implantation in mice. J Biol Chem 2002; 277:29260–29267.
46. Douglas NC, Tang H, Gomez R, Pytowski B, Hicklin DJ, Sauer CM, Kitajewski J, Sauer MV, Zimmermann RC. Vascular endothelial growth factor receptor 2 (VEGFR-2) functions to promote uterine decidual angiogenesis during early pregnancy in the mouse. Endocrinology 2009; 150:3845–3854.
47. Hayashi K, Erikson DW, Tilford SA, Bany BM, Maclean JA, Rucker EB III, Johnson GA, Spencer TE. *Wnt* genes in the mouse uterus: potential regulation of implantation. Biol Reprod 2009; 80:989–1000.
48. Large MJ, DeMayo FJ. The regulation of embryo implantation and endometrial decidualization by progesterone receptor signaling. Mol Cell Endocrinol 2012; 358:155–165.
49. Bevilacqua EM, Abrahamsohn PA. Trophoblast invasion during implantation of the mouse embryo. Arch Biol Med Exp (Santiago) 1989; 22: 107–118.
50. Chappell JC, Wiley DM, Bautch VL. Regulation of blood vessel sprouting. Semin Cell Dev Biol 2011; 22:1005–1011.
51. Halder JB, Zhao X, Soker S, Paria BC, Klagsbrun M, Das SK, Dey SK. Differential expression of VEGF isoforms and VEGF(164)-specific receptor neuropilin-1 in the mouse uterus suggests a role for VEGF(164) in vascular permeability and angiogenesis during implantation. Genesis 2000; 26:213–224.
52. Napp LC, Augustynik M, Paesler F, Krishnasamy K, Woiterski J, Limbourg A, Bauersachs J, Drexler H, Le NF, Limbourg FP. Extrinsic notch ligand delta-like 1 regulates tip cell selection and vascular branching morphogenesis. Circ Res 2012; 110:530–535.
53. Fantin A, Vieira JM, Gestri G, Denti L, Schwarz Q, Prykhozhij S, Peri F, Wilson SW, Ruhrberg C. Tissue macrophages act as cellular chaperones for vascular anastomosis downstream of VEGF-mediated endothelial tip cell induction. Blood 2010; 116:829–840.
54. Styp-Rekowska B, Hlushchuk R, Pries AR, Djonov V. Intussusceptive angiogenesis: pillars against the blood flow. Acta Physiol (Oxf) 2011; 202: 213–223.
55. Burke SD, Barrette VF, Bianco J, Thorne JG, Yamada AT, Pang SC, Adams MA, Croy BA. Spiral arterial remodeling is not essential for normal blood pressure regulation in pregnant mice. Hypertension 2010; 55:729–737.